Applied and Computational Mathematics
2024; 13(6): 211-223
http://www.sciencepublishinggroup.com/j/acm
doi: 10.11648/j.acm.20241306.11
ISSN: 2328-5605 (Print); ISSN: 2328-5613 (Online)

Mathematical Modelling of Multiphase Hybrid Gyro-tactic Nanofluid Flow Through Porous Convergent Pipe with Injection and Suction Using BVP4c

Chepkonga David, Mathew Kinyanjui, Roy Kiogora, Kang'ethe Giterere

Department Pure and Applied Mathematics, Jomo Kenyatta University of Agriculture and Technology, Nairobi, Kenya

Email address:

chepkonga.david@jkuat.ac.ke (Chepkonga David)
*Corresponding author

To cite this article:

Chepkonga David, Mathew Kinyanjui, Roy Kiogora, Kang'ethe Giterere. (2024). Mathematical Modelling of Multiphase Hybrid Gyro-tactic Nanofluid Flow Through Porous Convergent Pipe with Injection and Suction Using BVP4c. *Applied and Computational Mathematics, 13*(6), 211-223. https://doi.org/10.11648/j.acm.20241306.11

Received: 23 July 2024; **Accepted:** 2 September 2024; **Published:** 18 December, 2024

Abstract: This research focuses on enhancing fluid mobility by optimizing heat transfer, a crucial aspect in various industrial applications, including oil recovery. The study introduces an innovative framework that integrates microorganisms, hybrid nanoparticles, non-Newtonian fluid properties, a power law model, and inclined magnetic fields. The underlying dynamics are described by nonlinear partial differential equations, which are converted to ordinary differential equations using similarity transformation and subsequently solved through the BVP4c method. Key results demonstrate that fluid velocity increases with higher Reynolds, Hartman, Thermal Grashof, and Mass Grashof numbers due to factors such as reduced viscous drag, the Lorentz force's acceleration effect, and enhanced buoyancy. On the other hand, a higher Prandtl number slightly reduces velocity, while an increased Schmidt number raises it by steepening the velocity gradient. Regarding temperature, higher Reynolds and Prandtl numbers, along with increased Eckert and Radiation parameters, result in elevated fluid temperatures due to enhanced convective heat transfer, decreased thermal diffusivity, viscous dissipation, and radiative heat effects. The insights gained from this study are valuable for improving oil extraction efficiency by identifying and manipulating key parameters that affect fluid behavior.

Keywords: Multiphase, Hybrid, Gyro-tactic, Numerical Solution, Nanofluid, BVP4c

1. Introduction

The study of multiphase hybrid gyro-tactic nanofluid flow through porous convergent pipes with injection and suction holds significant relevance in both theoretical and applied fluid dynamics. These complex systems are pivotal in numerous industrial and engineering applications, including enhanced oil recovery, biomedical engineering, and advanced thermal management in electronic devices. The addition of nanofluids-fluids containing nanoparticles suspended in a base fluid-introduces marked improvements in thermal conductivity and heat transfer capabilities, offering a superior alternative to conventional fluids. This enhanced performance is particularly critical in environments where precise thermal control is necessary, such as microelectronics and medical devices.

Moreover, the integration of gyrotactic microorganisms into these nanofluids introduces an additional layer of complexity and potential benefits. Gyrotactic microorganisms, which orient themselves in response to fluid flow and gravity, can create unique bioconvective patterns that further enhance heat and mass transfer within the fluid. These characteristics make the study of such systems not only a subject of academic interest but also of considerable practical value.

The application of numerical methods, such as the BVP4c function in MATLAB, is instrumental in analyzing these intricate fluid dynamics. BVP4c, designed for solving boundary value problems for ordinary differential equations, provides a robust framework for conducting precise numerical simulations. These simulations are essential for understanding the multifaceted interactions within the fluid, such as

the effects of nanoparticle concentration, magnetic fields, and microorganism behavior on the overall flow and heat transfer properties. By leveraging these computational tools, researchers can optimize the performance of hybrid nanofluids in real-world applications, ultimately leading to more efficient and effective industrial processes.

Nazeer et al. [1] carried out numerical solution of gyrotactic microorganism flow of nanofluid over a Riga plate with the characteristics of chemical reaction and convective condition. They used Runge-Kutta method together with shooting technique to track the brownian motion of microorganisms. They took into account chemical reaction so as to aid thermophoresis of the nanoflow. They found that shear stress at the walls and the movement of microorganisms are significantly influenced by magnetic parameters.

Alsaedi et al. [2] carried out magnetohydrodynamics stratified bioconvection flow of nanofluid due to gyrotactic microorganisms. Microorganisms were used to stabilise the suspended nanoparticles through bioconvection. They used Homotopy method to solve the model. They remarked that Homotopy analysis method ensures the convergence of the series solutions. They noted that the velocity profiles decreases with increase in Hartman number. Increase in Peclet number and Lewis number, leads to an increase in the velocity profiles.

Jawad et al. [3] carried out a novel computational study on magnetohydrodynamics flow of nanofluid flow with gyrotactic microorganisms due to porous stretching sheet. They transformed the partial differential equations to ordinary differential equations using similarity transformation. The ODEs were solved using the package ND-solve on mathematica, and was numerically intergrated using shooting method. They noted that the field of microorganisms decreases by raising the value of bioconvection and peclet number.

Khan et al. [4] explored heat transfer enhancement in nanofluids using the Darcy-Forchheimer model, employing both analytical and numerical solutions. Their results indicated improved heat transfer rates in the presence of a magnetic field and thermal radiation, with applications in energy storage systems and cooling technologies.

sheikholes et al. [5] conducted a study on MHD nanofluid flow in porous cavities using numerical simulations with the finite difference method. They found that convection heat transfer is significantly enhanced under magnetic fields and heat flux boundary conditions, which can be applied in cooling systems for electronics and MHD power generation.

Kotnurkar & Giddaiah [6] studied bioconvection second grade Nanofluid flow containing Nanoparticles and Gyrotactic microorganisms. The governing partial differential equations were transformed into a system of ordinary differential equations using similarity variables and solved analytically using Homotopy analysis method. The microorganisms concentration diminished for the Brownian motion parameter and schmidt number, while it increased for the second grade nanofluid parameter. The temperature reduced with increase in Prandtl number, while it increased with increase in thermophoresis parameter and Lewis number.

Ahmad et al. [7] carried out a study on Nanofluid flow comprising Gyrotactic microorganisms through a porous medium. They noted that the dispersal of microorganisms in nanofluids improves heat transfer. The porous medium was also remarked to contribute to thermal efficiency. The governing equations were numerically solved by using successive over relaxation parameter method. The insertion of the gyrotactic microorganisms in the suspensions is widely used in the bio-microsystems. The gyrotactic microorganisms improved the stability of the nanofluid. The results proved beneficial in improving the efficiency of microbial fuel cells and heat transfer devices.

Pandey et al. [8] studied radiative heat transfer in stretching cylinders with nanofluids using analytical solutions with similarity transformations. Their findings demonstrated that radiation enhances heat transfer in nanofluid flow over stretching cylinders, relevant for manufacturing processes and energy systems.

Recent advancements in the mathematical modeling of multiphase hybrid gyro-tactic nanofluid flow have addressed various aspects of fluid behavior in porous media. One notable study focused on ternary hybrid nanofluids containing gyrotactic microorganisms flowing over different geometries, such as flat plates, wedges, and cones. Utilizing the Cattaneo¨CChristov model and solving with the BVP4c method, the research revealed that the geometrical configuration significantly influences heat and mass transfer rates, with cone geometries exhibiting the highest heat transfer (Moh, et al.) [9].

Another significant contribution explored non-Newtonian hybrid nanofluids under the influence of magnetic fields within porous media. This research highlighted how the Hartmann number, indicative of magnetic field strength, enhances fluid velocity due to the Lorentz force, offering valuable insights for optimizing cooling systems and magnetic field-based industrial applications (Lisha & Vijaya) [10].

The impact of suction and injection on hybrid nanofluid flow through porous media was examined, revealing that these processes significantly affect velocity and temperature profiles. The study demonstrated that suction decreases boundary layer thickness, leading to improved heat transfer efficiency, which is critical in thermal management systems (Moh, et al.) [9].

Research on the role of gyrotactic microorganisms in non-Newtonian nanofluids provided further insight, showing that these microorganisms enhance both velocity and temperature profiles, thereby improving heat and mass transfer. This finding is particularly relevant for applications in bioconvection and microbial fuel cells, where efficient transfer rates are essential (Lisha & Vijaya) [10].

The effects of magnetohydrodynamics (MHD) on hybrid nanofluid flow in porous media were also investigated, with results indicating that magnetic fields can be effectively used to control and enhance heat transfer, making this study pertinent to the design of advanced cooling systems (Moh, et al.) [9].

Another study explored how the shape of nanoparticles influences the flow and heat transfer properties of hybrid nanofluids. It was found that platelet-shaped nanoparticles provided the highest heat transfer rates, while spherical

nanoparticles offered the best balance between thermal conductivity and fluid flow. These insights are crucial for optimizing thermal systems in various industries (Moh, et al.) [9].

Chepkonga et al. [11], investigated fluid flow through collapsible tubes, the governing non linear equations were first transformed to ordinary differential equation using similarity transformation before being implemented in Matlab BVP4C solver. It was seen that the flow parameters significantly influence the flow properties.

Finally, the effects of thermal radiation on hybrid nanofluid flow in porous media were analyzed, revealing that thermal radiation significantly enhances temperature profiles, which is vital for high-temperature applications, particularly in aerospace and industrial processes (Moh, et al.) [9].

These studies collectively advance our understanding of how various factors, including geometrical configurations, magnetic fields, suction, injection, and thermal radiation, influence the behavior of hybrid nanofluids. This knowledge is essential for optimizing fluid flow and heat transfer in a range of industrial applications, from oil recovery to aerospace engineering.

Despite significant advancements in the study of multiphase hybrid gyro-tactic nanofluid flow through porous media, a comprehensive understanding of the combined effects of non-Newtonian fluids, hybrid nanoparticles, microorganisms, and inclined magnetic fields remains elusive. Existing research has predominantly focused on individual components such as gyrotactic microorganisms, magnetic fields, or nanofluids in isolation, often utilizing distinct methodologies like the Runge-Kutta method, Homotopy analysis, or similarity transformations for simplified geometries and conditions. There is a notable research gap in systematically integrating these elements within a single, coherent model to capture their synergistic interactions accurately. Furthermore, the potential of leveraging inclined magnetic fields in enhancing the heat transfer and mobility of such complex fluid systems has been underexplored. Addressing these gaps could lead to optimized strategies for enhanced oil recovery and other industrial applications, providing a more robust framework for future experimental and computational studies in this domain.

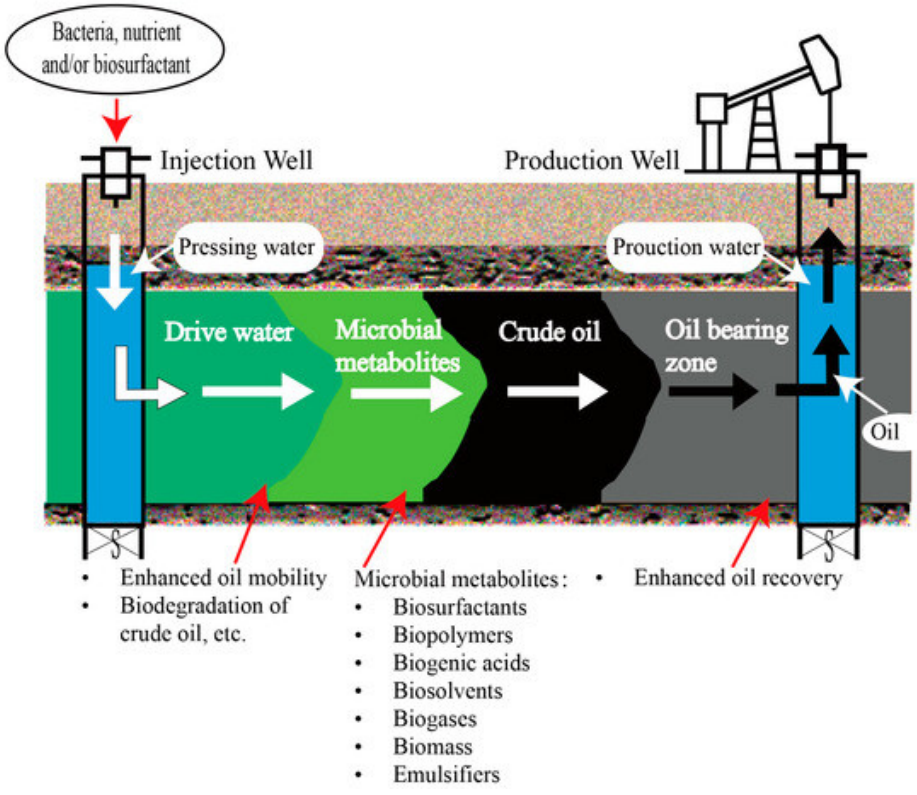

Figure 1. *Flow Geometry.*

2. Mathematical Formulation

This study investigates the flow dynamics within a porous convergent pipe, focusing on a stratified two-layer scenario involving an incompressible fluid and Gyro-tactic microorganisms, as depicted in Figure 2. The upper half of the pipe contains an Oil phase while the lower half contains water. The flow is characterized as laminar and unsteady, with viscosity varying nonlinearly due to temperature gradients and tangential directions in both phases. The energy driving the fluid flow includes viscous dissipation, thermal radiation, and chemical reactions, with thermal conductivity exhibiting temperature-dependent changes.

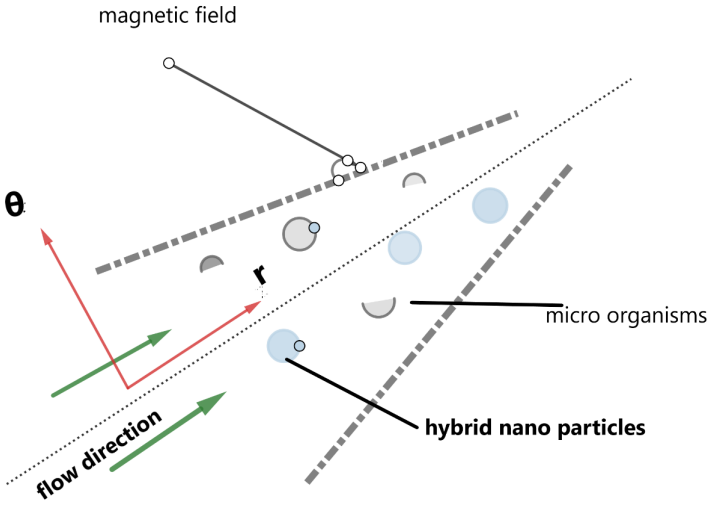

Figure 2. *Computational Domain.*

2.1. The Effective Properties of Hybrid Nanofluid

The study focuses on a hybrid nanofluid denoted as $Cu - Al_2O_3 - H_2O/OIL, Cu - Al_2O_3 - H_2O/OIL$. Employing the pseudo-single phase approach, this methodology treats the composite of water and oil as a singular fluidic entity. This pseudo-fluid is characterized by averaging relevant physical properties of water and oil. The properties considered include dynamic viscosity, density, heat capacity, thermal expansion coefficient, thermal conductivity, and electrical conductivity. These properties, extensively utilized in similar research such as by [12], are summarized as follows:

$$\mu_{hnf} = \mu_f(1-\phi_1)^{-2.5}(1-\phi_2)^{-2.5} \tag{1}$$

$$\frac{\rho_{hnf}}{\rho_f} = (1-\phi_2)\left[(1-\phi_1) + \phi_1\frac{\rho_1}{\rho_f}\right] + \phi_2\frac{\rho_2}{\rho_f} \tag{2}$$

$$\frac{(\rho C_p)_{hnf}}{(\rho C_p)_f} = (1-\phi_2)\left[(1-\phi_1) + \phi_1\frac{(\rho C_p)_1}{(\rho C_p)_f}\right] + \phi_2\frac{(\rho C_p)_2}{(\rho C_p)_f} \tag{3}$$

$$\frac{(\rho\beta)_{hnf}}{(\rho\beta)_f} = (1-\phi_2)\left[(1-\phi_1) + \phi_1\frac{(\rho\beta)_1}{(\rho\beta)_f}\right] + \phi_2\frac{(\rho\beta)_2}{(\rho\beta)_f} \tag{4}$$

$$\frac{k_{hnf}}{k_{bf}} = \frac{k_2 + 2k_{bf} - 2\phi_2(k_{bf}-k_2)}{k_2 + 2k_{bf} + \phi_2(k_{bf}-k_2)} \tag{5}$$

$$\frac{k_{bf}}{k_f} = \frac{k_1 + 2k_f - 2\phi_1(k_f-k_1)}{k_1 + 2k_f + \phi_1(k_f-k_1)} \tag{6}$$

$$\frac{\sigma_{hnf}}{\sigma_{bf}} = \frac{\sigma_2 + 2\sigma_{bf} - 2\phi_2(\sigma_{bf}-\sigma_2)}{\sigma_2 + 2\sigma_{bf} + \phi_2(\sigma_{bf}-\sigma_2)} \tag{7}$$

$$\frac{\sigma_{bf}}{\sigma_f} = \frac{\sigma_1 + 2\sigma_f - 2\phi_1(\sigma_f-\sigma_1)}{\sigma_1 + 2\sigma_f + \phi_1(\sigma_f-\sigma_1)} \tag{8}$$

This study addresses the comprehensive modeling of oil, water, hybrid nanoparticles, and microorganisms through a set of fundamental equations: continuity, momentum conservation, energy conservation, concentration, and microorganism density. The momentum equation is enriched by incorporating a magnetic field at an angle, buoyancy force driving flow dynamics, a Darcy-type source term to account for porosity effects, and a variable viscosity formulation that considers non-linear variations with temperature and direction. The energy equation is extended to include internal heating via viscous dissipation, joule heating due to induced electric currents influenced by magnetic fields, and thermal radiation effects to capture electromagnetic radiation phenomena. Additionally, the concentration equation incorporates chemical reactions and thermophoresis, providing a comprehensive framework to model the behavior of hybrid nanofluids in complex flow scenarios. These advancements significantly enhance our ability to simulate and understand the intricate dynamics of such multiphase systems, contributing valuable insights to the field of fluid dynamics and heat transfer in heterogeneous media.

2.2. Equation of Continuity

$$\frac{\partial}{\partial r}(ru_r) = 0 \tag{9}$$

2.3. Equation of Conservation of Momentum

$$\rho_{hnf}\left[\frac{\partial \vec{u}}{\partial t} + \vec{u}\cdot(\vec{\nabla}\vec{u})\right] = -\vec{\nabla}P + \vec{\nabla}\cdot\vec{\tau} + \rho_{hnf}\vec{F} \tag{10}$$

2.4. Equation of Energy

$$(\rho C_p)_{hnf}\left[\frac{\partial T}{\partial t} + \vec{V}\cdot(\vec{\nabla}T)\right] = \vec{\nabla}\cdot k_{hnf}\vec{\nabla}T + S \tag{11}$$

2.5. Equation of Concentration

$$\frac{\partial C}{\partial t} + \vec{V}\cdot(\vec{\nabla}C) = D_{hnf}\vec{\nabla}^2 C + S_{hnf} \tag{12}$$

2.6. Equation of Microorganism Density

$$\frac{\partial N}{\partial t} + \vec{V}\cdot(\vec{\nabla}N) = D_m\vec{\nabla}^2 N \tag{13}$$

The boundary conditions for the multiphase flow is given by,
At the pipe wall, $\theta = \pm\alpha$

$$u_r = 0, u_\theta = u_o, T = T_w, C = C_w, N = N_w \tag{14}$$

At $\theta = 0$, the interface is treated as a moving wall.

$$u_r = u_\infty, u_\theta = 0, T = T_\infty, C = C_\infty, N = N_\infty \tag{15}$$

At $r = 0$

$$u_r = u_\infty, u_\theta = 0, T = T_\infty, C = C_\infty, N = N_\infty \tag{16}$$

At $r = \infty$, the gradients of all variables in the flow direction are zero as proposed by [13].

$$\frac{\partial u_\theta}{\partial r} = 0, \frac{\partial u_r}{\partial r} = 0, \frac{\partial T}{\partial r} = 0, \frac{\partial C}{\partial r} = 0, \frac{\partial N}{\partial r} = 0 \tag{17}$$

The equations 9, 10, 11, 12, and 13 are initially converted to the cylindrical coordinate system to align with the geometry of the computational domain. Subsequently, these transformed equations are subjected to a similarity transformation, thereby converting them into ordinary differential equations. This preparatory step is crucial before employing the Spectral method for numerical solution. By doing so, we optimize computational efficiency and accuracy, harnessing the method's robustness in addressing intricate boundary value problems effectively.

The similarity transforms used are;

$$u_r(\theta,t) = -\frac{Q}{r}\frac{1}{\delta^{m+1}}f(\eta), \frac{\omega(\eta)}{\delta^{m+1}} = \frac{T-T_w}{T_\infty - T_w}, \frac{\phi(\eta)}{\delta^{m+1}} = \frac{C-C_w}{C_\infty - C_w}, \frac{\Theta(\eta)}{\delta^{m+1}} = \frac{N-N_w}{N_\infty - N_w} \tag{18}$$

The transformations 18, transforms the equations 10, 11, 12 and 13. Additionally the thermophysical properties are applied to obtain;

$$[s(n-1)\{s(n-1)-1\}]\,\theta^{s(n-1)-2}\frac{B}{G}\left[-r^2 f' - \frac{r^3}{Q}\delta^{m+1}u_\theta\right] + \left[s(n-1)\theta^{s(n-1)-1}\right]\frac{B}{G}\left[-4f - r^2 f'' + 4rf + \frac{r^3}{k}f\right]$$

$$+\theta^{s(n-1)}A\left[-4rf' - r^2 f''' + \frac{r^3}{k}f' - \frac{r^2}{Q}u_\theta\delta^{m+1} + \frac{r^3\delta^{m+1}}{Da}\right] - (m+1)\frac{r^{m+2}}{\delta^{m+1}}\lambda f' + \frac{2r^2}{\delta^{m+1}}Reff' + rRef'' + rRef$$

$$+\frac{r}{Q}\sin\beta_1\left[Gr_{(T)}\omega'+Gr_{(C)}\phi'+Gr_{(N)}\Theta'\right]-\frac{r}{Q}\cos\beta_1\times\left[Gr_{(T)}\omega+Gr_{(C)}\phi+Gr_{(N)}\Theta\right]+Ha^2F(r\sin^2\alpha)f'=0 \quad (19)$$

$$\frac{1}{DB\,Pr}\left[C+C\,b+\frac{R}{k_fC}\right]\omega''+\frac{1}{Pr}\frac{bC}{DB}\frac{1}{\delta^{m+1}}(\omega')^2-\frac{r}{A}Re\omega'+\frac{(m+1)}{A}\frac{r^{m+1}}{\delta^{m+1}}\lambda\omega+\frac{Ec}{D}\left[\frac{4}{r^2\delta^{m+1}}f^2\right]$$
$$+\frac{Ec}{D}\left[\delta^{m+1}\frac{u_\theta^2}{Q^2}+\frac{2u_\theta}{rQ}f'+\frac{1}{r^2\delta^{m+1}}(f')^2\right]+\frac{F}{DB}\frac{Q^2}{\delta^{m+1}}Jf^2=0 \quad (20)$$

$$\frac{1}{A\,Sc}\phi''-\frac{Re}{A}\phi'+\frac{(m+1)}{A}\frac{r^{m+1}}{\delta^{m+1}}\lambda\phi-\frac{k_1}{Nt\delta^{m+1}+\omega}\times\left[-\left(\frac{Nc\delta^{m+1}+\phi}{Nt\delta^{m+1}+\omega)}\right)(\omega')^2\right]-\frac{k_1}{Nt\delta^{m+1}+\omega}$$
$$\times\left[(Nc+\phi)\left(\frac{Nt\delta^{m+1}+\omega}{Nt+\omega}\right)\omega''+\omega'\phi'\right]-\frac{\mu_0k_1}{Nt\delta^{m+1}+\omega}\left(Nc\delta^{m+1}+\phi\right)\left(B(n-1)s\theta^{s(n-1)-1}\right)(\omega')$$
$$-\frac{Kc}{A}Re\left(Nc\delta^{m+1}+\phi\right)=0 \quad (21)$$

$$\frac{Lb}{A}\Theta''-\frac{Re}{A}\Theta'-\frac{Pe}{B\,Lb}r\Theta'\phi'+\frac{(m+1)}{A}\frac{r^{m+1}}{\delta^{m+1}}\lambda\Theta-\frac{rPe}{A\,Lb}\left(Nn\delta^{m+1}+\Theta\right)\frac{1}{\delta^{m+1}}\phi''=0 \quad (22)$$

Transforming the boundary conditions 14, 15,16 and 17, using the transformations 18, we have
At $\theta=\pm\alpha$

$$f(\eta)=0,\omega=0,\phi=0,\Theta=0 \quad (23)$$

At $\theta=0$,

$$f(\eta)=-\frac{u_\infty r\delta^{m+1}}{Q},\omega=\delta^{m+1},\phi=\delta^{m+1},\Theta=\delta^{m+1} \quad (24)$$

At $r=0$

$$f(\eta)=-\frac{u_\infty r\delta^{m+1}}{Q},\omega=\delta^{m+1},\phi=\delta^{m+1},\Theta=\delta^{m+1} \quad (25)$$

At $r=\infty$

$$\frac{\partial f}{\partial r}=0,\frac{\partial\omega}{\partial r}=0,\frac{\partial\phi}{\partial r}=0,\frac{\partial\Theta}{\partial r}=0 \quad (26)$$

3. Numerical Solution

3.1. Reduction of Order of ODEs

The equations (19), (20), (21) and (22) together with the boundary conditions (23) to (26) are first reduced to one order less. It basically targets to reduce a higher-order ordinary differential equation to a first order ODE. This is basically done to simplify the problem and make it more managable to solve. The reduction of order technique is particularly useful when trying to solve homogenous ODEs.
The suitable substitutions in this case are

$$\begin{gathered}y_1=f,y_2=f',y_3=f'',y_3'=f'''\\ y_4=\omega,y_5=\omega',y_5'=\omega''\\ y_6=\phi,y_7=\phi',y_7'=\phi''\\ y_8=\Theta,y_9=\Theta',y_9'=\Theta''\end{gathered} \quad (27)$$

Substituting (27) into equation (19) we have,

$$y_1=f,$$
$$y_1'=y_2=f',$$
$$y_2'=y_3=f'',$$
$$y_3'=f'''=\frac{1}{A\,\theta^{s(n-1)}}\left\{-\frac{m+1}{\delta^{m+1}}r^m\lambda y_2+2\frac{Re}{\delta^{m+1}}y_1y_2+\frac{Re}{r}y_3+\frac{Re}{r}y_1+\frac{\sin\beta_1}{Qr}\left[Gr_{(T)}y_5+Gr_{(C)}y_7+Gr_{(N)}y_9\right]\right\}$$
$$+\frac{1}{\theta^{s(n-1)}}\left\{-\frac{\cos\beta_1}{Qr}\left[Gr_{(T)}y_3'+Gr_{(C)}y_5+Gr_{(N)}y_6\right]\right.$$

$$+\frac{F\ Ha^2\sin^2\alpha}{r}y_2\Bigg\}+\left[s(n-1)\{s(n-1)-1\}\right]\theta^{-2}\times\frac{B}{AG}\left[-y_2-\frac{r}{Q}\delta^{m+1}u_\theta\right]$$
$$+\left[s(n-1)\theta^{-1}\right]\frac{B}{AG}\left[-\frac{4}{r^2}y_1-y_3+\frac{4}{r}y_1+\frac{r}{k}y_1\right]+\left[-\frac{4}{r}y_2+\frac{r}{k}y_2-\frac{u_\theta}{Q}\delta^{m+1}+\frac{r\delta^{m+1}}{Da}\right] \tag{28}$$

Substituting (27) into equation (20) we have,

$$\begin{aligned}
&y_4=\omega,\\
&y_5=\omega',\\
&y_5'=\omega''=\frac{DB\ Pr}{\left[C+C\ b+\frac{R}{k_f\ C}\right]}\left\{\frac{-C\ b}{Pr\ DB\ \delta^{m+1}}y_5^2+\frac{rRe}{A}y_5-\frac{(m+1)r^{m+1}}{A\ \delta^{m+1}}\lambda y_4\right\}-\frac{DB\ Pr}{\left[C+C\ b+\frac{R}{k_f\ C}\right]}\left\{\frac{Ec}{D}\right.\\
&\left.\times\left[\frac{4}{r^2\delta^{m+1}}y_1^2+\frac{\delta^{m+1}u_\theta^2}{Q^2}+\frac{2u_\theta}{rQ}y_2+\frac{1}{r^2\delta^{m+1}}y_2^2\right]-\frac{F}{DB}\frac{Q^2}{\delta^{m+1}}Jy_1^2\right\}
\end{aligned} \tag{29}$$

Substituting (27) into equation (21) we have,

$$\begin{aligned}
&y_6=\phi,\\
&y_7=\phi',\\
&y_7'=\phi''=A\ Sc\left\{\frac{Re}{A}y_7-\frac{(m+1)}{A}\frac{r^{m+1}}{\delta^{m+1}}\lambda y_6+\frac{k_1}{Nt\delta^{m+1}+y_4}\times\left[-\left(\frac{Nc\delta^{m+1}+y_6}{Nt\delta^{m+1}+y_4}\right)y_5^2\right]\right\}\\
&\quad+A\ Sc\left\{\frac{k_1}{Nt\delta^{m+1}+y_4}\left[(Nc+y_6)\left(\frac{Nt\delta^{m+1}+y_4}{Nt+y_4}\right)y_5'\quad+y_5y_7\right]\right.\\
&\quad\left.+\frac{\mu_0k_1}{Nt\delta^{m+1}+y_4}\left[\left(Nc\delta^{m+1}+y_6\right)\left(B(n-1)s\times\theta^{s(n-1)-1}\right)y_5\right]\right\}+\frac{Kc}{A}Re\left(Nc\delta^{m+1}+y_6\right)
\end{aligned} \tag{30}$$

Substituting (27) into equation (22) we have,

$$\begin{aligned}
&y_8=\Theta,\\
&y_9=\Theta',\\
&y_9'=\Theta''=\frac{A}{Lb}\left\{\frac{Re}{A}y_9+\frac{Pe}{B\ Lb}ry_7y_9-\frac{(m+1)}{A}\frac{r^{m+1}}{\delta^{m+1}}\lambda y_8\right\}+\frac{A}{Lb}\left\{r\frac{Pe}{A\ Lb}\left(Nn\delta^{m+1}+y_8\right)\frac{1}{\delta^{m+1}}y_7'\right\}
\end{aligned} \tag{31}$$

3.2. Reduction of Order for Boundary Conditions

Substituting (27) into equations (23) to (26) we have,
At $\theta=\pm\alpha$ we have

$$f(\eta)=y_1=0,\omega=y_5=\delta^{m+1},\phi=y_8=\delta^{m+1},\Theta=\delta^{m+1} \tag{32}$$

At $\theta=0$ we have

$$f(\eta)=\frac{-u_\infty r\delta^{m+1}}{Q},\omega=y_4=0,\phi=y_6=0,\Theta=y_8=0 \tag{33}$$

At $r=0$ we have

$$f(\eta)=\frac{-u_\infty r\delta^{m+1}}{Q},\omega=y_4=0,\phi=y_6=0,\Theta=y_8=0 \tag{34}$$

As $r\to\infty$ we have

$$f(\eta)'=y_2=0,\omega'=y_5=0,\phi'=y_7=0,\Theta'=y_9=0 \tag{35}$$

3.3. Final Set of Governing Equations

The final set of governing equations together with the boundary conditions is given as

$$
\begin{cases}
y_2, \\
y_3, \\
y_3' = \frac{1}{A\ \theta^{s(n-1)}}\left\{ -\frac{m+1}{\delta^{m+1}} r^m \lambda y_2 + 2\frac{Re}{\delta^{m+1}} y_1 y_2 + \frac{Re}{r} y_3 + \frac{Re}{r} y_1 + \frac{\sin\beta_1}{Qr}\left[Gr_{(T)} y_5 + Gr_{(C)} y_7 + Gr_{(N)} y_9\right] \right\} \\
\quad + \frac{1}{\theta^{s(n-1)}}\left\{ -\frac{\cos\beta_1}{Qr}\left[Gr_{(T)} y_4 + Gr_{(C)} y_6 + Gr_{(N)} y_8\right] + \frac{F\ Ha^2 \sin^2\alpha}{r} y_2 \right\} \\
\quad + \left[s(n-1)\{s(n-1)-1\}\right]\theta^{-2}\frac{B}{AG}\left[-y_2 - \frac{r}{Q}\delta^{m+1} u_\theta\right] + \left[s(n-1)\theta^{-1}\right]\frac{B}{AG}\left[-\frac{4}{r^2} y_1 - y_3 + \frac{4}{r} y_1 + \frac{r}{k} y_1\right] \\
\quad + \left[\frac{-4}{r} y_2 + \frac{r}{k} y_2 - \frac{u_\theta}{Q}\delta^{m+1} + \frac{r\delta^{m+1}}{Da}\right], \\
y_5, \\
y_5' = \frac{DB\ Pr}{\left[C + C\ b + \frac{R}{k_f\ C}\right]}\left\{ \frac{-C\ b}{Pr\ DB\ \delta^{m+1}} y_5^2 + \frac{rRe}{A} y_5 - \frac{(m+1) r^{m+1}}{A\ \delta^{m+1}} \lambda y_4 \right\} \\
\quad - \frac{DB\ Pr}{\left[C + C\ b + \frac{R}{k_f\ C}\right]}\left\{ \frac{Ec}{D}\left[\frac{4}{r^2\delta^{m+1}} y_1^2 + \frac{\delta^{m+1} u_\theta^2}{Q^2} + \frac{2u_\theta}{rQ} y_2 + \frac{1}{r^2\delta^{m+1}} y_2^2\right] - \frac{F}{DB}\frac{Q^2}{\delta^{m+1}} J y_1^2 \right\}, \\
y_7, \\
y_7' = A\ Sc\left\{ \frac{Re}{A} y_7 - \frac{(m+1)}{A}\frac{r^{m+1}}{\delta^{m+1}} \lambda y_6 + \frac{k_1}{Nt\delta^{m+1} + y_4} \times \left[-\left(\frac{Nc\delta^{m+1} + y_6}{Nt\delta^{m+1} + y_4}\right) y_5^2 \right] \right\} \\
+ A\ Sc\left\{ \frac{k_1}{Nt\delta^{m+1} + y_4}\left[(Nc + y_6)\left(\frac{Nt\delta^{m+1} + y_4}{Nt + y_4}\right) y_5' + y_5 y_7 \right] \right. \\
\left. + \frac{\mu_0 k_1}{Nt\delta^{m+1} + y_4}\left[\left(Nc\delta^{m+1} + y_6\right) \times \left(B(n-1) s\theta^{s(n-1)-1}\right) y_5 \right] \right\} + \frac{Kc}{A} Re\left(Nc\delta^{m+1} + y_6\right), \\
y_9, \\
y_9' = \frac{A}{Lb}\left\{ \frac{Re}{A} y_9 + \frac{Pe}{B\ Lb} r y_7 y_9 - \frac{(m+1)}{A}\frac{r^{m+1}}{\delta^{m+1}} \lambda y_8 \right\} + \frac{A}{Lb}\left\{ r\frac{Pe}{A\ Lb}\left(Nn\delta^{m+1} + y_8\right)\frac{1}{\delta^{m+1}} y_7' \right\}
\end{cases}
\tag{36}
$$

$$
\begin{cases}
y_1 = 0, y_4 = \delta^{m+1}, y_6 = \delta^{m+1}, y_8 = \delta^{m+1} \text{ at } \theta = \pm\alpha \\
y_1 = \frac{-u_\infty r\delta^{m+1}}{Q}, y_2 = 0, y_4 = 0, y_6 = 0, y_8 = 0 \text{ at } \theta = 0 \\
y_1 = \frac{-u_\infty r\delta^{m+1}}{Q}, y_4 = 0, y_6 = 0, y_8 = 0 \text{ at } r = 0 \\
y_2 = 0, y_5 = 0, y_7 = 0, y_9 = 0 \text{ as } r \to \infty
\end{cases}
\tag{37}
$$

3.4. Results

The systems of equations (36) together with the boundary conditions (37) were implemented in BVP4c, inbuilt function in MATLAB, and the results were visualized through graphs. These graphical representations are comprehensively discussed as follows:

3.5. Effects of Flow Parameters on Velocity

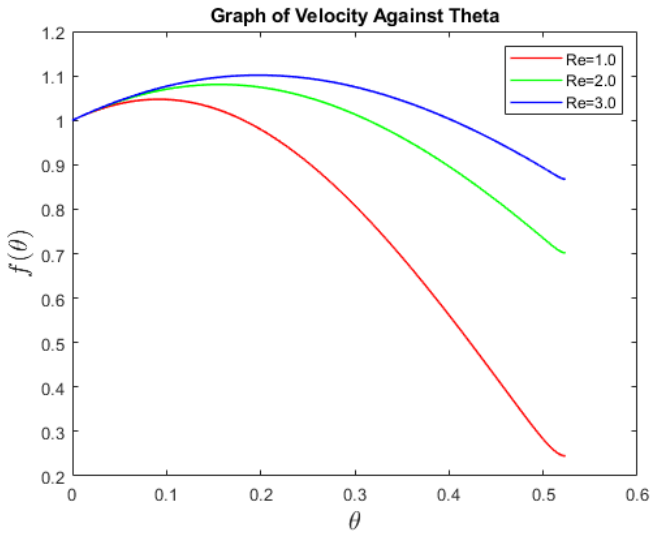

Figure 3. *Graph of velocity for varying Reynolds Number.*

From Figure 3, it is evident that an increase in the Reynolds number results in a higher fluid velocity. This behavior can be attributed to the corresponding decrease in viscous forces with an increasing Reynolds number. As the fluid experiences reduced viscosity, it encounters less resistance to flow, thereby facilitating a faster movement.

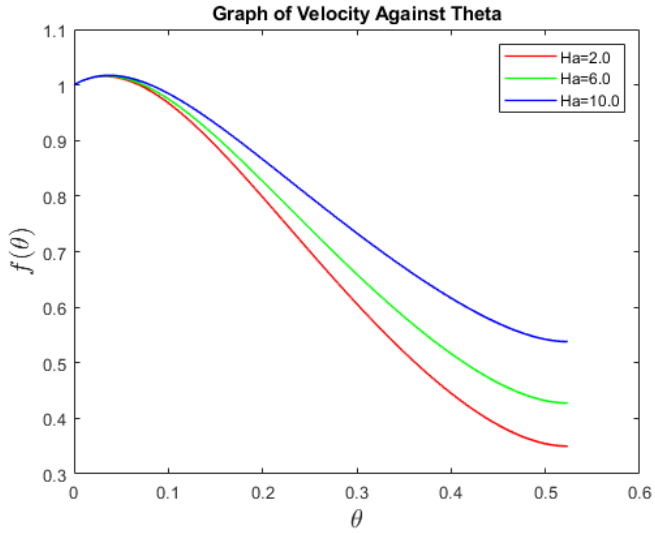

Figure 4. *Graph of velocity for varying Hartman Number.*

From Figure 4, it is observed that an increase in the Hartman number enhances the velocity profile. The magnetic field, applied at an angle to the fluid flow, generates a Lorentz force. This force accelerates the fluid, resulting in increased velocity. The acceleration is particularly effective because the angled application of the magnetic field enhances the fluid's movement.

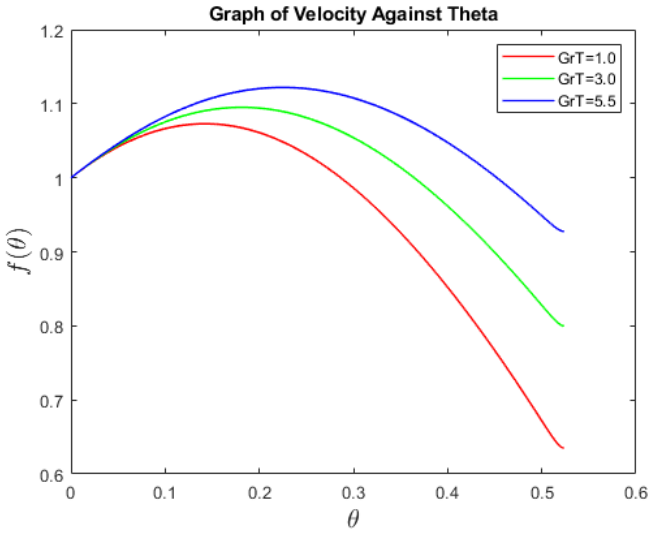

Figure 5. *Graph of velocity for varying Thermal Grashof Number.*

From Figure 5, it is evident that an increase in the Thermal Grashof number leads to higher velocity profiles. This occurs because the Thermal Grashof number quantifies the buoyancy force relative to viscous forces in the fluid. As the Thermal Grashof number increases, buoyancy forces become more significant, driving the fluid to move faster and thus increasing the velocity profiles.

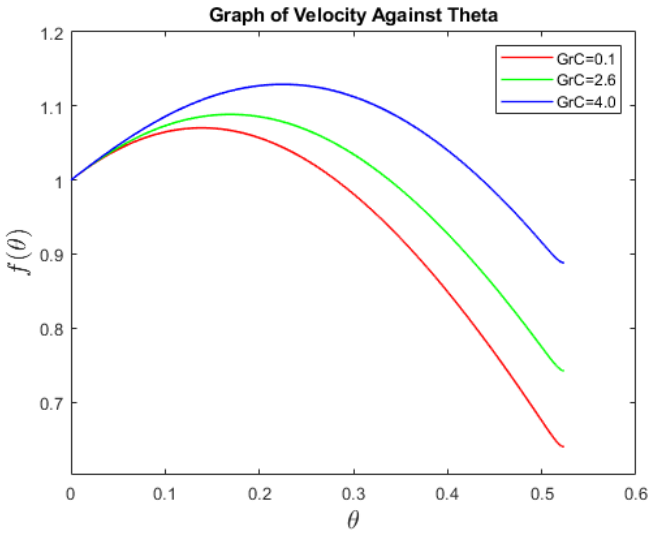

Figure 6. *Graph of velocity for varying Mass Grashof Number.*

From Figure 6, it is evident that an increase in the mass Grashof number results in higher velocity profiles. The mass Grashof number measures the ratio of buoyancy forces due to concentration differences to viscous forces. As the mass Grashof number increases, the buoyancy forces become more dominant, causing the fluid to accelerate and resulting in increased velocity profiles.

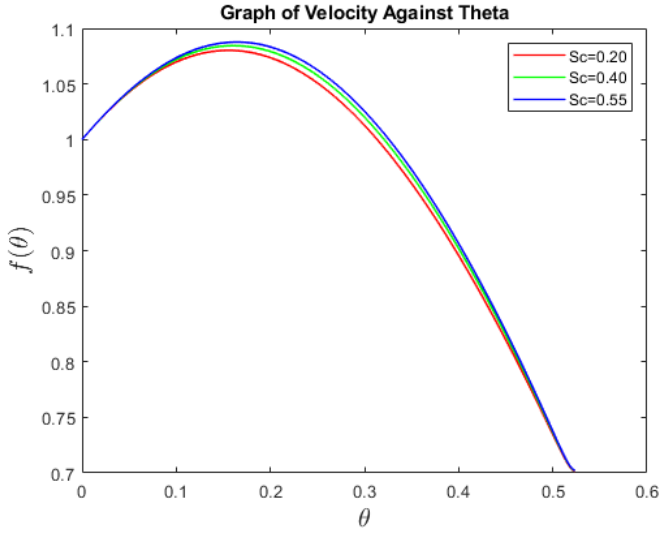

Figure 7. *Graph of velocity for varying Schmidt Number.*

From Figure 7, it is observed that an increase in the Schmidt number leads to higher velocity profiles. The Schmidt number is the ratio of viscous diffusion rate to mass diffusion rate. A higher Schmidt number indicates lower mass diffusivity, meaning the momentum diffuses more slowly compared to the concentration. This results in a steeper velocity gradient and, consequently, an increase in velocity profiles.

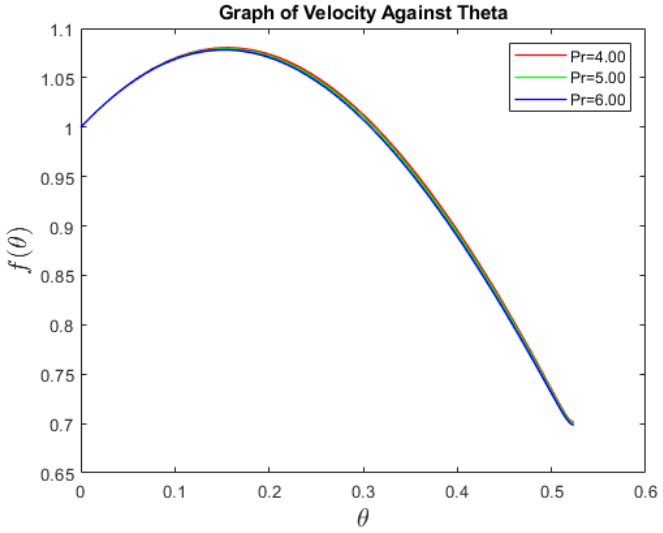

Figure 8. *Graph of velocity for varying Prandtl Number.*

From Figure 8, it can be seen that an increase in the Prandtl number leads to a slight decrease in the velocity profile. Although the change is gradual, this trend occurs because the Prandtl number represents the ratio of momentum diffusivity to thermal diffusivity. A higher Prandtl number indicates lower thermal diffusivity relative to momentum diffusivity, which reduces the rate at which heat spreads compared to momentum. This reduction in thermal diffusion results in a decrease in the velocity profile, albeit gradually.

3.6. Effects of Flow Parameters on Temperature

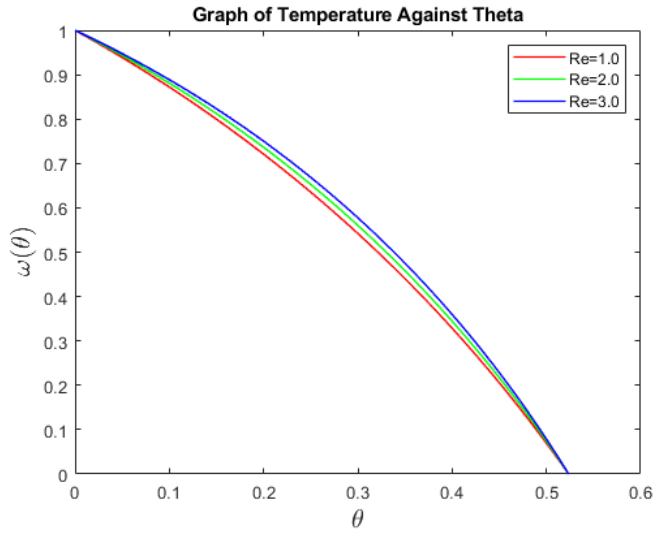

Figure 9. *Graph of temperature for varying Reynolds number.*

From Figure 9, it is observed that an increase in the Reynolds number results in a higher fluid temperature. This occurs because a higher Reynolds number indicates a more turbulent flow, which enhances convective heat transfer within the fluid. Increased turbulence promotes better mixing and more efficient heat distribution, leading to a rise in the fluid's temperature.

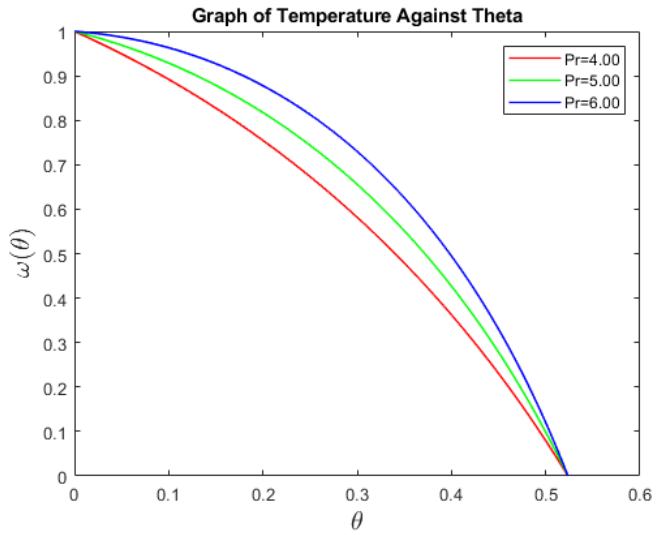

Figure 10. *Graph of temperature for varying Prandtl Number.*

From Figure 10, it is observed that an increase in the Prandtl number leads to a rise in the fluid temperature. The Prandtl number is the ratio of momentum diffusivity (kinematic viscosity) to thermal diffusivity. A higher Prandtl number indicates that thermal diffusivity is relatively low compared to momentum diffusivity. This means that heat transfers less efficiently through the fluid compared to momentum.

Consequently, with a higher Prandtl number, heat tends to accumulate more in the fluid, resulting in an increase in the temperature profile.

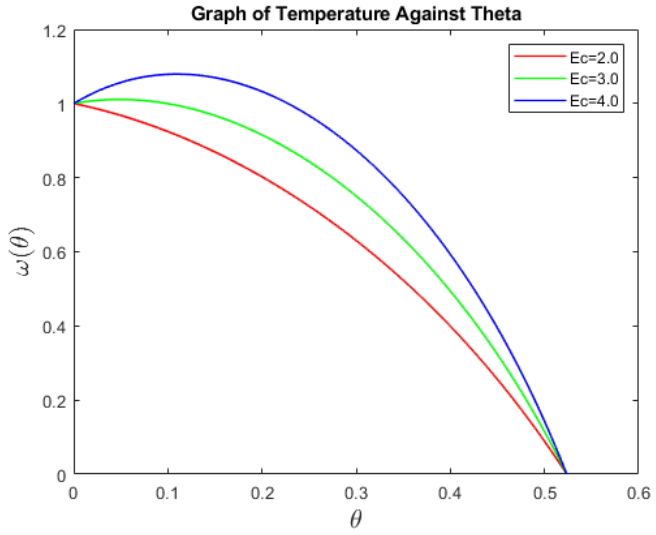

Figure 11. *Graph of temperature for varying Eckert Number.*

From Figure 11, it is evident that an increase in the Eckert number leads to a rise in the fluid temperature. The Eckert number is a dimensionless number that quantifies the relative importance of viscous dissipation to thermal energy in the fluid. As the Eckert number increases, it indicates that the energy generated by viscous dissipation (due to frictional forces within the fluid) becomes more significant compared to the thermal energy. This additional energy input from viscous dissipation contributes to an increase in the fluid's temperature.

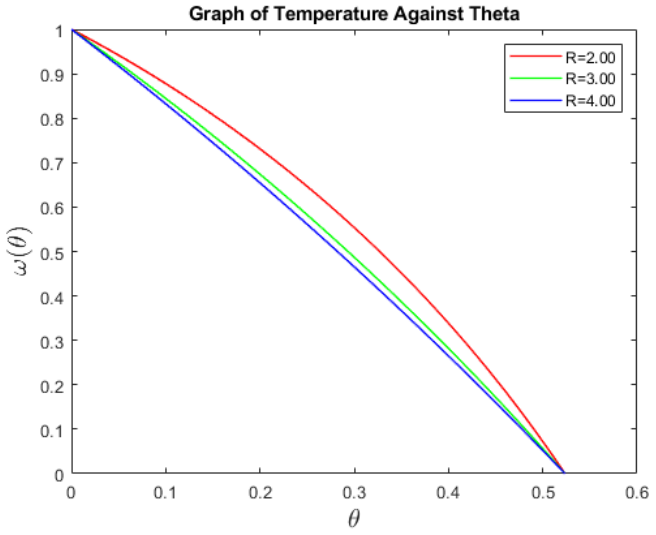

Figure 12. *Graph of temperature for varying Radiation Parameter.*

From Figure 12, it is observed that an increase in the Radiation parameter results in a higher fluid temperature. The Radiation parameter quantifies the relative significance of radiative heat transfer compared to conductive and convective heat transfer. A higher Radiation parameter indicates that radiative heat transfer becomes more dominant. As radiation contributes additional thermal energy to the fluid, it enhances the overall heat content, leading to an increase in the fluid's temperature.

4. Conclusion

The key findings of this research are:

1. *Reynolds Number and Velocity:* It was observed that higher Reynolds numbers substantially increase fluid velocity, primarily due to the reduction in viscous resistance. This is a crucial factor in applications requiring efficient fluid movement, such as in pipeline transport and cooling systems.
2. *Hartman Number and Velocity:* The enhancement of fluid velocity with an increased Hartmann number highlights the significant role of the Lorentz force in accelerating fluid flow under magnetic fields. This finding is particularly relevant for magnetic fluid applications, including magnetic drug delivery and electromagnetic pumps.
3. *Thermal Grashof Number and Velocity:* The study demonstrated that higher Thermal Grashof numbers effectively boost velocity profiles by amplifying buoyancy forces relative to viscous forces. This result is vital for optimizing natural convection processes in thermal management systems.
4. *Mass Grashof Number and Velocity:* Similarly, an increase in mass Grashof numbers leads to higher velocities due to stronger buoyancy forces from concentration differences. This phenomenon can be leveraged in enhanced oil recovery techniques, where buoyancy-driven flows are essential for efficient extraction.
5. *Schmidt Number and Velocity:* The research showed that a higher Schmidt number steepens the velocity gradient by decreasing mass diffusivity, thereby raising velocity profiles. This insight is useful for applications involving mass transfer, such as in chemical reactors and separation processes.
6. *Prandtl Number and Velocity:* The study found that a higher Prandtl number slightly decreases velocity profiles due to reduced thermal diffusivity relative to momentum diffusivity. Understanding this relationship is crucial for systems where precise thermal and flow control is necessary.
7. *Reynolds Number and Temperature:* Higher Reynolds numbers were found to increase fluid temperature, primarily due to enhanced convective heat transfer driven by increased turbulence. This finding underscores the importance of Reynolds number control in heat exchangers and cooling technologies.
8. *Prandtl Number and Temperature:* Increased Prandtl numbers were shown to lead to higher fluid temperatures, as lower thermal diffusivity causes heat

to accumulate. This result is particularly relevant for designing systems that require efficient heat retention, such as in thermal storage devices.

9. *Eckert Number and Temperature:* The study revealed that higher Eckert numbers result in increased temperature due to greater viscous dissipation, which contributes to thermal energy. This effect is important for high-energy applications where managing viscous heating is critical.
10. *Radiation Parameter and Temperature:* Finally, the research indicated that a higher Radiation parameter increases fluid temperature by adding more thermal energy through radiative heat transfer. This finding has implications for high-temperature industrial processes, where radiation effects must be carefully managed.

4.1. General Recommendations

1. *Optimization of Flow Parameters*: Optimize parameters such as Reynolds number, Hartmann number, and Grashof numbers based on specific applications to achieve desired fluid dynamics outcomes, like enhanced heat transfer or controlled flow behavior.
2. *Integration of Magnetic Fields*: Consider incorporating magnetic fields to increase flow rates in applications where electromagnetic control can enhance system performance, such as in magnetic drug targeting or cooling systems.
3. *Temperature Control Through Radiative and Viscous Effects*: Carefully control the Radiation parameter and Eckert number in thermal management systems to ensure precise temperature regulation, which is critical in microelectronics and biomedical devices.

4.2. Recommendations for Engineers

1. *Design of Heat Exchangers and Cooling Systems*: Engineers should take into account the influence of Reynolds and Prandtl numbers when designing heat exchangers and cooling systems. Higher Reynolds numbers can enhance convective heat transfer, while the Prandtl number should be optimized to balance thermal and momentum diffusivity.
2. *Application of Magnetic Fields in Fluid Flow Systems*: Utilize the enhancement of fluid velocity through increased Hartmann numbers by exploring magnetic fields in fluid flow systems, such as magnetic refrigeration or electromagnetic pumps, to optimize flow performance.
3. *Enhanced Oil Recovery (EOR) Techniques*: Consider increasing both thermal and mass Grashof numbers to amplify buoyancy forces, improving the efficiency of oil extraction processes in enhanced oil recovery (EOR) applications.
4. *Advanced Thermal Management*: Control the Radiation parameter in high-temperature environments like aerospace or industrial furnaces to effectively manage radiative heat transfer and prevent overheating.
5. *Customization of Nanofluid Properties*: Tailor nanofluid properties, including nanoparticle concentration and base fluid type, based on desired Schmidt and Prandtl numbers to achieve optimal fluid dynamics, especially in designing specialized cooling fluids or lubricants in mechanical systems.

Acknowledgments

The authors would like to thank the School of Mathematical and Physical Sciences for the support given.

Conflicts of Interest

The authors wish to declare no conflicts of interest regarding the publication of this research article.

References

[1] M. Nazeer, S. Saleem, F. Hussain, and M. U. Rafiq, "Numerical solution of gyrotactic microorganism flow of nanofluid over a Riga plate with the characteristic of chemical reaction and convective condition," *Waves in Random and Complex Media*, pp. 1-23, 2022.

[2] A. Alsaedi, M. I. Khan, M. Farooq, N. Gull, and T. Hayat, "Magnetohydrodynamic (MHD) stratified bioconvective flow of nanofluid due to gyrotactic microorganisms," *Advanced Powder Technology*, vol. 28, no. 1, pp. 288-298, 2017.

[3] M. Jawad, K. Shehzad, and R. Safdar, "Novel computational study on MHD flow of nanofluid flow with gyrotactic microorganism due to porous stretching sheet," *Punjab University Journal of Mathematics*, vol. 52, no. 12, 2021.

[4] S. U. Khan, S. A. Shehzad, and N. Ali, "Darcy-Forchheimer MHD couple stress liquid flow by oscillatory stretched sheet with thermophoresis and heat generation/absorption," *Journal of Porous Media*, vol. 21, no. 12, 2018.

[5] M. Sheikholeslami, S. Shehzad, Z. Li, and A. Shafee, "Numerical modeling for alumina nanofluid magnetohydrodynamic convective heat transfer in a permeable medium using Darcy law," *International Journal of Heat and Mass Transfer*, vol. 127, pp. 614-622, 2018.

[6] N. S. Khan, "Bioconvection in second grade nanofluid flow containing nanoparticles and gyrotactic microorganisms," *Brazilian Journal of Physics*, vol. 48, no. 3, pp. 227-241, 2018.

[7] S. Ahmad, M. Ashraf, and K. Ali, "Nanofluid flow comprising gyrotactic microorganisms through a porous medium," *Journal of Applied Fluid Mechanics*, vol. 13, no. 5, pp. 1539-1549, 2020.

[8] A. K. Pandey and M. Kumar, "Natural convection and thermal radiation influence on nanofluid flow over a stretching cylinder in a porous medium with viscous dissipation," *Alexandria Engineering Journal*, vol. 56, no. 1, pp. 55-62, 2017.

[9] M. Yaseen, S. K. Rawat, N. A. Shah, M. Kumar, and S. M. Eldin, "Ternary hybrid nanofluid flow containing gyrotactic microorganisms over three different geometries with Cattaneo-Christov model," *Mathematics*, vol. 11, no. 5, p. 1237, 2023.

[10] N. Lisha and A. Vijaya Kumar, "Mixed bio-convection analysis on MHD Casson hybrid nanofluid flow over a spinning cone/plate embedded in a variable porosity medium: A comparative study," *The European Physical Journal Plus*, vol. 138, no. 11, p. 1042, 2022.

[11] D. Chepkonga, R. Kiogora, and K. Giterere, "Fluid flow and heat transfer through a vertical cylindrical collapsible tube in the presence of magnetic field and an obstacle," *International Journal of Advances in Applied Mathematics and Mechanics*, vol. 71, pp. 62-71, 2019.

[12] M. N. Othman, A. Jedi, and N. A. A. Bakar, "MHD flow and heat transfer of hybrid nanofluid over an exponentially shrinking surface with heat source/sink," *Applied Sciences*, vol. 11, no. 17, p. 8199, 2021.

[13] A. Mavi and T. Chinyoka, "Finite volume computational analysis of the heat transfer characteristic in a double-cylinder counter-flow heat exchanger with viscoelastic fluids," in *Defect and Diffusion Forum*, vol. 424, pp. 19-43, Trans Tech Publ, 2023.